JOURNAL OF SOLID STATE CHEMISTRY 91, 375–384 (1991)

Thermal Behavior and Oxidation Mechanism of Tetragonal Manganite Spinels $Cu_xMn_{3-x}O_4$, $0 < x < 1$

B. GILLOT AND M. KHARROUBI

Laboratoire de Recherches sur la Réactivité des Solides associé au CNRS Faculté des Sciences Mirande, B. P. 138-21004, Dijon Cedex, France

AND R. METZ, R. LEGROS, AND A. ROUSSET

Laboratoire de Chimie des Matériaux Inorganiques, Université Paul Sabatier Toulouse 111, 118, route de Narbonne, 31062 Toulouse Cedex, France

Received October 16, 1990; in revised form November 28, 1990

In the present work, the oxidation mechanism and cationic distribution of the single phase copper manganite spinels $Cu_xMn_{3-x}O_4$ ($0 < x < 1$) prepared by thermal processing of copper–manganese-coprecipitated hydroxide precursors have been investigated in the temperature range 300–900°C. Thermogravimetry measurements and infrared spectrometry have enabled us to propose copper and manganese ion distributions in the spinel lattice which are given by the formula $(Cu_x^+ Mn_{1-x}^{2+})_A(Mn_{2-x}^{3+}Mn^{4+})_BO_4^{2-}$ when the oxidation temperature is lower for Cu^+ ions than that for Mn^{2+} ions. Further, isothermal oxidations achieved below 450°C showed, for composition $x > 0.70$, the formation of cation-deficient spinels with oxidation kinetics controlled by a diffusion law. With decreasing of copper content, the kinetic curves become sigmoidal according to nucleation growth-mechanism induced by the formation of α-Mn_2O_3. © 1991 Academic Press, Inc.

Introduction

Much research has been carried out to elucidate the structure and properties of Ni–Cu manganite spinels (*1–3*). Some of these studies have focused on the transport properties of $CuMn_2O_4$ alone (*4–6*) or Ni–Cu manganites $Mn_{7/3-x}Cu_xNi_{2/3}O_4$ ($x > 0.40$), for example in relation to their application as NTC thermistor components (*7, 8*). However, up to now, less attention has been directed toward the problem of how to improve the thermal stability in an air atmosphere which is of considerable importance for both understanding the oxidation mechanism as a function of temperature and technological applications of the low resistivity NTC. In addition, it has been found that copper manganese oxides were powerful oxidation catalysts in the combustion of organic compounds (*9*). In particular, amorphous $CuMn_2O_4$ presents in oxygen a redox-controlled charge exchange $Cu^{2+} + Mn^{3+} \rightleftarrows Cu^+ + Mn^{4+}$, which has been suggested to play a vital role in catalyst activity (*10*).

Therefore, we undertook the present work to clarify the oxidoreduction mechanism for solid solutions $CuMn_2O_4$–Mn_3O_4 when the presence of certain variable cat-

0022-4596/91 $3.00

ions that also change the electrical properties (*11*) complicates the behavior in various atmospheres of the manganese mixed oxides (*12*). Such a change is principally caused by oxidation during which the valence of the cations increases and induces the spinal phase decomposition when the oxidation is achieved above 500°C for powders prepared by a standard ceramic route (*13*) under conditions of utilization as a thermistor material. Some important clues to the thermal stability in oxygen and cationic distribution were obtained from the investigation by means of thermogravimetry and infrared spectrometry.

Experimental

The conditions of preparation of $Cu_xMn_{3-x}O_4$ spinels with $0 < x < 1$ and the characterization (differential thermal analysis, X-ray diffraction, electrical conductivity, morphology) have already been published in Ref. (*13*). Thermal decomposition in air of coprecipitated mixed copper manganese hydroxydes does not lead directly to single spinel phase formation. Instead, the decomposition at 700°C results in a mixture of phase comprising Mn_2O_3 and $Cu_{1.5}Mn_{1.5}O_4$. After 700°C, a mass loss due to the reduction of these oxides was observed. Then, in the range 900 to 1200°C, the solid solution $Cu_xMn_{3-x}O_4$ appeared with a slight presence of Mn_3O_4 phase. These features have been rationalized according to the equation:

$$(3 - 2x)/2Mn_2O_3 + 2x/3Cu_{1.5}Mn_{1.5}O_4 \rightarrow x/(x + \alpha)Cu_{x+\alpha}Mn_{3-(x+\alpha)}O_4 \ldots + \alpha(x + \alpha Mn_3O_4 + (3 - 2x)/12O_2,$$

where $\alpha \ll x$.

To obtain single phase spinels with $Cu_xMn_{3-x}O_4$ with $0 \ll x \ll 1$, the Mn–Cu coprecipitated hydroxide precursors were decomposed at 700°C to yield powders which were pressed into disk form of 8 mm diameter and 5 mm thickness under 5×10^8 Pa. These pressed disks were submitted to heat treatment in air, with different profiles, as depicted in Table 1, to yield the single-phase spinels. Such treatment at high temperature has been found to cause an increase of the crystallite size since the average diameter observed from electron microscopy was on the order of 2 to 3 μm.

TABLE 1

CHARACTERISTICS OF THE $Cu_xMn_{3-x}O_4$ SPINELS

Sample x	c/a	Heat treatment temperature in °C	Time in hours
0.96	1.048	900	48
0.86	1.066	910	48
0.75	1.086	980	48
0.45	1.134	1100	48
0.31	1.150	1200	48
0.11	1.163	1200	24
0	1.165	1250	4

It has been established from XRD analysis (*13*) that the decrease of tetragonal distortion observed for copper manganite spinels (Table 1) can only be explained by the two ionic configurations $(Cu_x^+ Mn_{1-x}^{2+})_A (Mn_{2-x}^{3+} Mn_x^{4+})_B O_4^{2-}$ or $(Cu_x^{2+} Mn_{1-x}^{2+})_A (Mn_2^{3+})_B O_4^{2-}$ with copper ions at the A sites. Moreover, conductivity measurements throughout the range $0 < x < 1$, indicated a maximum conductivity for $x = 1$ (*11*) that supports the ionic configuration $(Cu_x^+ Mn_{1-x}^{2+})_A (Mn_{2-x}^{3+} Mn_x^{4+})_B O_4^{2-}$ with a maximum number of Mn^{3+}–Mn^{4+} pairs for $x = 1$ which contribute to the conduction through a hopping mechanism.

The oxidations were performed under nonisothermal or isothermal conditions in a Setaram MTB 10-8 microbalance using 6 mg of ground powder. Before every isothermal oxidation, great care had to be taken while degassing to ensure that the powder was not even partially oxidized. This necessitated a

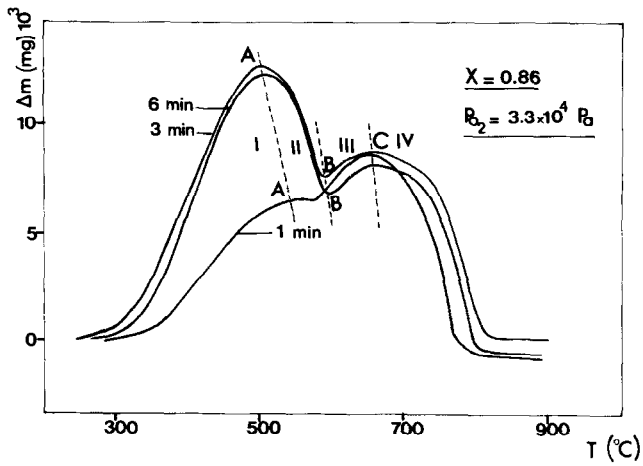

FIG. 1. TG curves showing the effect of grinding time on oxidation behavior for a spinel with $x = 0.86$.

vacuum of 10^{-3} Pa and a very slow temperature rise, during which time no mass change occurred.

Infrared spectra in transmission mode were recorded using a double beam Perkin–Elmer 580B spectrophotometer. Samples for IR examination were prepared by dry grinding (with agate mortar and pestle), a mixture of 1 mg of sample dispersed in 200 mg of CsI of spectroscopic grade. All the spectra were obtained at room temperature in the range 900–200 cm^{-1}. The oxidation degree of the samples at various levels of reaction were calculated from the gravimetric data.

Results and Discussion

Nonisothermal Oxidation

Figures 1 and 2 show the main results concerning the effect of grinding time and oxygen partial pressure on the mass variation Δm when a copper–manganite spinel with the composition $x = 0.86$ was heated at a constant rate of 2.5°C min^{-1} from 200 to 900°C. Concerning the grinding time, the zero time represents the duration below which mass change could not be detected by thermogravimetry. It can be observed, as can be expected, that longer grinding times and higher oxygen pressures lead to a greater reaction rate and oxidized amount. As the amount of reacting oxygen and hence the monitored mass change is sensitive to grinding and equilibrium oxygen fugacity, a systematic study was made concerning the grinding duration and the oxygen partial pressure in order to obtain a maximum mass gain for each composition. This maximum mass gain defined "the optimum conditions" invoked in the text. The change in shape of these curves with increasing oxidation temperature permits the discerning of four regions for samples with $x > 0.75$ (Fig. 3, curves a and b), particularly a mass loss between 500 and 600°C (region II). Above 700°C (region IV), TGA curves are also characterized by a domain of reduction that restores the initial stoichiometry of the samples. The regions I and II correspond to an oxidation which depends on copper content.

Figure 4 presents the results on the grinding time dependence on the mass variation

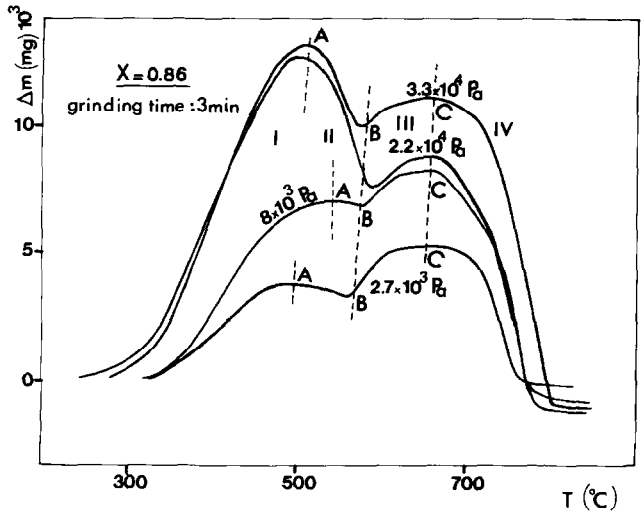

FIG. 2. TG curves showing the effect of oxygen pressure on oxidation behavior for a spinel with $x = 0.86$.

Δm for a sample with $x = 0.45$ heated under an oxygen pressure of 3.3×10^4 Pa and Fig. 5 shows the effect of oxygen pressure for a sample ground 5 min for $x = 0.75$. Again, the oxidized amount increases with increasing grinding time or oxygen pressure but for these compositions three regions can be seen since the two oxidations (regions I and III) are not separated by a reduction region but only by a break in the $m = f(T)$ curves. For this composition range, XRD analysis of samples heated at 900°C indicates the reappearance of a spinel phase associated with sudden mass loss in the TG curves. A similar behavior is also observed for other compositions with $x < 0.75$ (Fig. 3, curves c, d, e, and f).

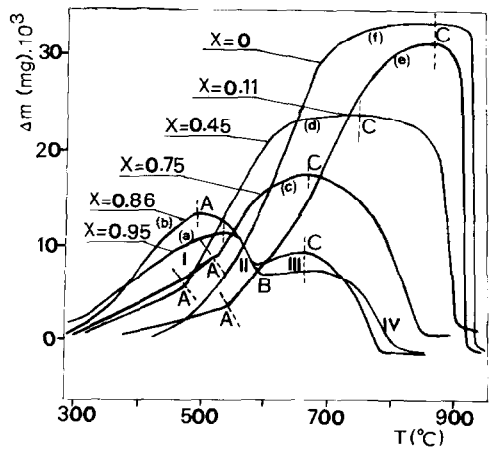

FIG. 3. TG curves for copper manganite spinels for optimum conditions (grinding time and oxygen pressure).

It may be noted from Fig. 3 that for optimum conditions (grinding time and oxygen pressure) the temperature as well as the intensity of the second peak of oxidation (region III, point C) gradually increases with manganese concentration. From previous studies concerning the oxidation of manganese mixed oxides with spinel structure when the mass change above 550°C is also due to oxidation of Mn^{2+} ions located in *A*-sites (*14*), the mass gain observed above 600°C can therefore be attributed to the oxidation of Mn^{2+} ions into Mn^{3+} ions located in *A*-sites of the spinel lattice. The low-temperature oxidation step starting at 300°C and extending up to a maximum of around 500°C

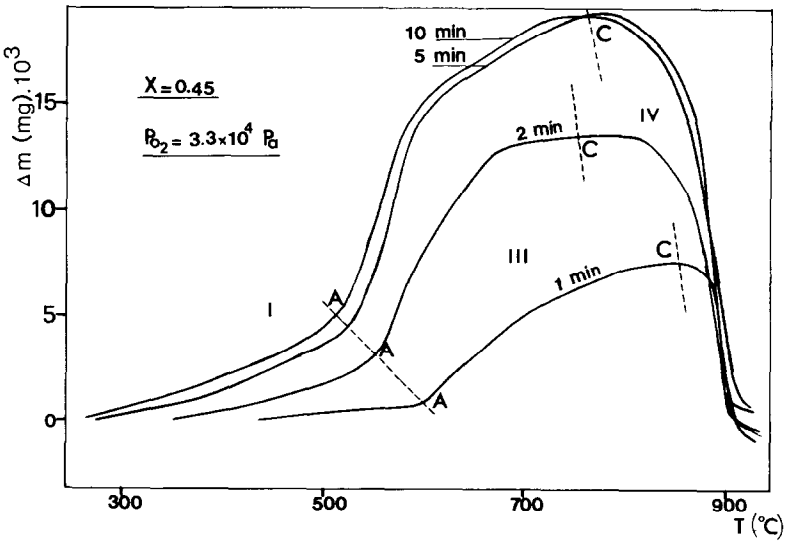

FIG. 4. TG curves showing the effect of grinding time on oxidation behavior for a spinel with $x = 0.45$.

is principally due to the oxidation of Cu^+ ions. The fact that in the case of the nickel manganites $Ni_xMn_{3-x}O_4$ which possess Mn^{2+} ions at their *A*-sites as the lone oxidizable cation the oxidation temperature is above 500°C (*12*), permits us to attribute in the copper manganites the phenomenon appearing at low temperature to the oxidation of Cu^+ ions to Cu^{2+} ions. As expected the intensity of the first peak (point A) increases with copper content while the second peak (point C) diminishes with increasing x in accordance with the increasing substitution of tetrahedral Mn^{2+} ions by Cu^+ ions.

In order to clarify this oxidation, a detailed study was made by X-ray diffraction of samples heated at temperatures corresponding to the maximum of mass gain (point A on Fig. 3 for $x > 0.75$ and point C for $x < 0.75$) for 1 hr and quenched. Powder XRD analyses of the oxidation products indicate the existence of α-Mn_2O_3 and a cubic spinel phase. The spinel phase is identified as $CuMn_2O_4$ or $Cu_{1.5}Mn_{1.5}O_4$ but because of the close similarities between the structures of these two spinels (*15*, *16*), it was not possible to identify the exact nature of the compound solely from XRD patterns. Therefore, we have envisaged initially two

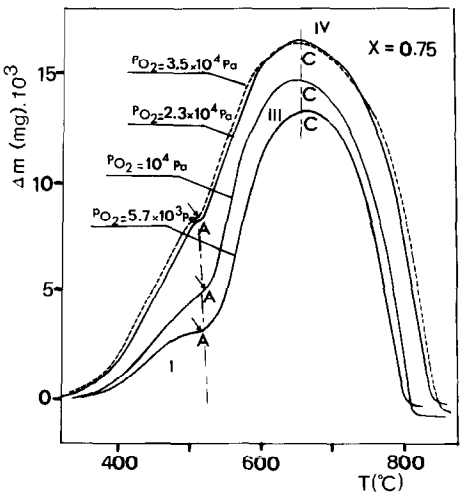

FIG. 5. TG curves showing the effect of oxygen pressure on oxidation behavior for a spinel with $x = 0.75$.

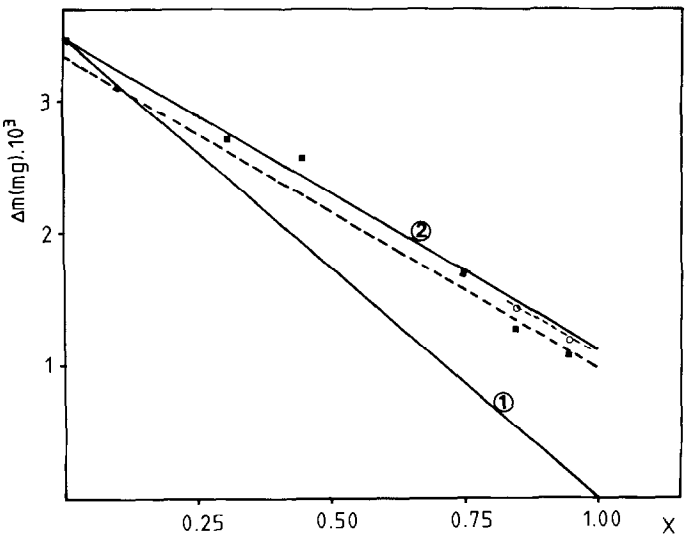

FIG. 6. Evolution of experimental mass gain (---) and theoretical mass gain (—) for Reactions (1) and (2).

oxidation reactions leading to a spinel phase and α-Mn_2O_3:

$$Cu_xMn_{3-x}O_4 + (1 - x)/2O_2 \rightarrow 3(1 - x)Mn_2O_3 + xCuMn_2O_4 \quad (1)$$

with a mass gain of $\Delta P = (8 - 8x)/(8.6x + 228.81)$ and

$$Cu_xMn_{3-x}O_4 + (3 - 2x)/12O_2 \rightarrow (3 - 2x)/2Mn_2O_3 + \tfrac{2}{3}xCu_{1.5}Mn_{1.5}O_4 \quad (2)$$

with a mass gain of $\Delta P = (24 - 16x)/(25.83x + 686.37)$.

Figure 6 represents the theoretical calculated mass gain from Formulae (1) and (2) as a function of copper content. Figure 6 shows also the experimental mass gain at points A and C. The experimental mass gain is found to follow Reaction (2) as shown by a good correlation between the experimental points and the calculated curve. However, for $x > 0.75$ a better agreement is obtained if we also consider the oxidized amount of Mn^{2+} ions corresponding to region III (amount BC on Fig. 5 and circles open on Fig. 6).

These observations are in agreement with results obtained from electrical measurements (*11*, *13*) and support the following cation distribution:

$$(Mn^{2+}_{1-x}Cu^{+}_{x})_A(Mn^{3+}_{2-x}Mn^{4+}_{x})_BO^{2-}_4 .$$

The oxidation mechanism may then be depicted by the following reaction:

$$(Cu^{+}_{x}\,Mn^{2+}_{1-x})_A(Mn^{3+}_{2-x}Mn^{4+}_{x})_BO^{2-}_4 - (3 - 2x)/12O_2 \rightarrow \tfrac{3}{2}x(Cu^{+})_A(Cu^{2+}_{0.5}Mn^{4+}_{1.5})_BO^{2-}_4 + (3 - 2x)/2\alpha\text{-}Mn_2O_3 . \quad (3)$$

This distribution suggested the contribution of two oxidation reactions compatible with:

$$xCu^{+} \rightarrow x/3Cu^{2+} + 2x/3Cu^{+} \quad (4)$$

with the oxidation of $\frac{1}{3}$ of the Cu^{+} ions and

$$(1 - x)Mn^{2+} + (2 - x)Mn^{3+} \rightarrow (3 - 2x)Mn^{3+} \quad (5)$$

with the total oxidation of the Mn^{2+} ions.

The "plateau" region or the break observed in Figs. 3 and 4 (point A) can be

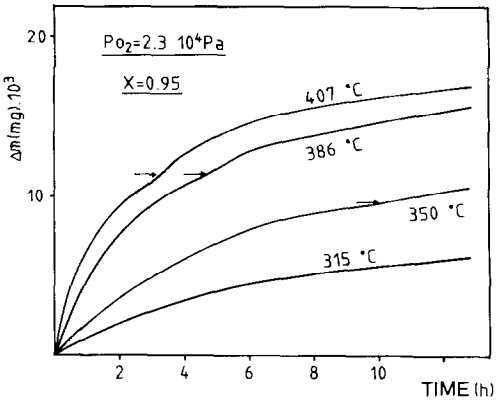

FIG. 7. Kinetic curves, $\Delta m = f(t)$, for spinel with $x = 0.95$.

regarded as being caused by the difference in the reactivity of Cu^+ and Mn^{2+} located on *A*-sites of the spinel structure. The value of partial mass gain calculated at point A and that increases with copper content corresponds well to the oxidation of $\frac{1}{3}$ of the Cu^+ ions. The mass loss observed in the range 500–600°C for $x > 0.75$ can be considered due, as in the case of manganese substituted magnetites, to the reduction of a certain proportion of the Mn^{4+} ions (*14*).

Since the oxidation temperature for Cu^+ ions is lower than that of Mn^{2+} ions, it should be possible to characterize more thoroughly the oxidation mechanism by the isothermal oxidation method at relatively low temperature through the formation of metastable cation-deficient spinels as intermediate phases (*14*).

Isothermal Oxidation

The oxidation kinetics relative to region I for samples with compositions $x = 0.95$ and $x = 0.75$ are depicted in Figs. 7 and 8. These curves display a two-stage oxidadion process for $T > 350$°C. The initial pattern shows that the reaction starts immediately with a maximum rate, the amount oxidized (shown by an arrow) being similar to that obtained under nonisothermal conditions (Fig. 3, point A for $x = 0.95$ and C for $x = 0.75$). The additional mass gain observed above 350°C and the dependence of the reaction time can be attributed to a partial oxidation of Mn^{3+} into Mn^{4+} ions. These curves are consistent with a diffusion-controlled process involving a composition gradient through particles leading below 450°C to the formation of a cation-deficient spinel phase (*12*). In order to verify this presumption an attempt was made to differentiate the formed phases on the basis of their IR spectra during the isothermal oxidations. In contrast to the spectrum of unoxidized spinel (Fig. 9, curve a), all the spectra of the samples with $x > 0.70$ oxidized between 300 and 450°C showed the presence of a large number of absorption bands (Fig. 9, curves b and c), suggesting an octahedral ordering. Order–disorder phenomena in spinels have a great influence on the IR absorption spec-

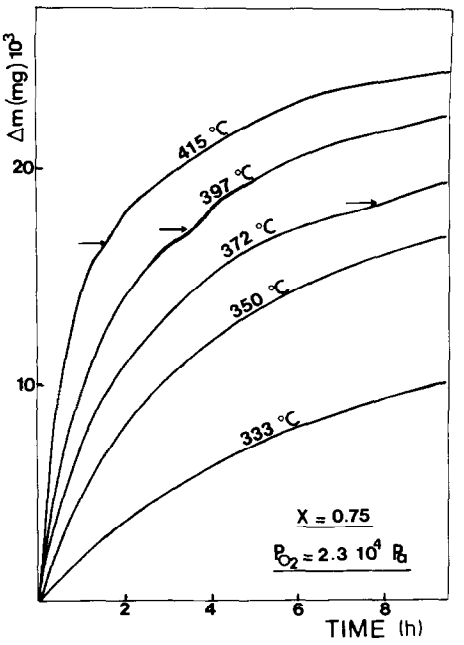

FIG. 8. Kinetic curves, $\Delta m = f(t)$, for spinel with $x = 0.75$.

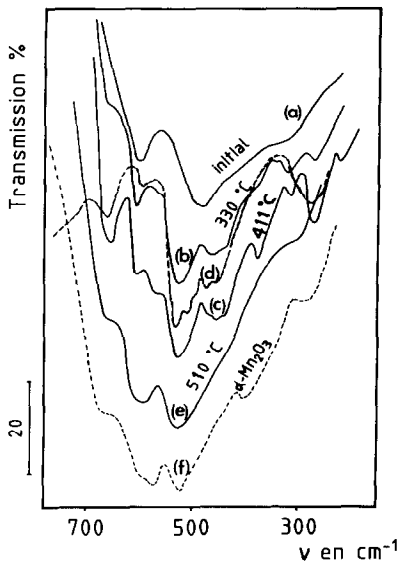

FIG. 9. Infrared absorption spectra of spinel with $x = 0.75$ heated at different temperatures under isothermal conditions. Curve d: IR spectrum of ordered $Cu_{1.5}Mn_{1.5}O_4$ [Ref. (*15*)].

tra (*17*). A 1 : 3 ordering on the B sublattice reduces the space group from O_h^7 to O^7 and according to White *et al.* (*18*) the number of IR active modes increases from 4 to 21, which gives rise to a fine structure in the IR spectrum.

A close similarity was observed between the IR spectra of our samples with that given in the literature for ordered $CuMg_{0.5}Mn_{1.5}O_4$ (*16*) or $Cu_{1.5}Mn_{1.5}O_4$ at 360°C (*15, 19*) (Fig. 9, curve d). In the X-ray diffraction pattern of $CuMg_{0.5}Mn_{1.5}O_4$, Blasse (*20*) found superstructure lines indicating a 1 : 3 octahedral ordering. The superstructure lines in the X-ray diffraction pattern for $Cu_{1.5}Mn_{1.5}O_4$ could not be found, which is obviously because of the close X-ray scattering power of Cu and Mn. A further proof for 1 : 3 ordering on the B-sites was found by neutron diffraction (*21*). The only possibility for this ordering is that the cation valencies and distributions are given by:

$$(Cu^+)_A(Mg^{2+}_{0.5}Mn^{4+}_{1.5})_BO_4^{2-}$$
$$\text{and } (Cu^+)_A(Cu^{2+}_{0.5}Mn^{4+}_{1.5})_BO_4^{2-},$$

which favors the Cu(*A*)–Mn(*B*) ground state. It might be concluded that the ionic order is of the same kind, i.e., 1 : 3 order on *B*-sites, which supports Eq. (3). Therefore, the proposed cation-deficient spinel obtained by isothermal oxidation below 450°C arises through the oxidation reaction:

$$\begin{aligned}(Cu_x^+ Mn^{2+}_{1-x})_A(Mn^{3+}_{2-x}Mn_x^{4+})_BO_4^{2-} \\ + (3 - 2x + 3y)/12O_2 \rightarrow \\ (3 - 2x - y)/2\gamma\text{-}Mn_2^{3+}O_3^{2-} \\ + t/24(Cu^+_{16x/t})_A(Cu^{2+}_{8x/t}Mn^{4+}_{24(x+y)/t\square\beta)})_BO_4^{2-},\end{aligned} \quad (6)$$

where $\beta = 3y/t$, $t = 16x + 9y$, and $\square$ and y represent the vacancies of cations and the oxidation content of Mn^{3+} ions, respectively.

In comparison with the spinel obtained before the additional mass gain [Reaction (3)] in which the Mn^{4+}/Cu^{2+} ratio in *B*-sites favors an ordering phenomenon, it can be observed that this ratio changes slightly for cation-deficient spinels if y remains low, which would explain the preservation of the ordering.

Unfortunately the superstructure line in the X-ray diffraction pattern for the cation-deficient spinel could not be found, which is due to the similar X-ray scattering power of Cu and Mn. Concerning the presence of Mn_2O_3 that accompanied the cation-deficient spinel, it should be considered that oxidation will rather take place through the segregation of γ-Mn_2O_3 instead of α-Mn_2O_3, which results in broadening of the X-ray diffraction lines as observed experimentally. The former modification of Mn_2O_3 has a spinel structure where vacancies are mainly located on *A*-sites and can be attributed to the clustering of the distorting Jahn–Teller ions like Mn^{3+}, which plays an important role in the stability and the homo-

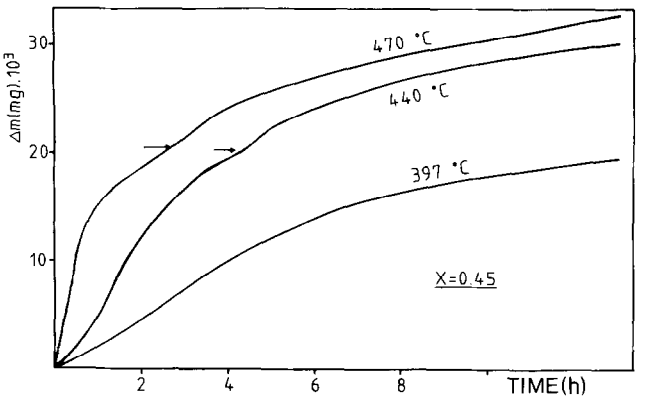

FIG. 10. Kinetic curves, $\Delta m = f(t)$, for spinel with $x = 0.45$.

geneity of the spinel structure (*16*). From the IR spectra of the samples heated at 330 and 411°C, additional absorption bands at 320 and 380 cm^{-1} are observed. Comparison between these additional bands and those of γ-Mn_2O_3 (*22*) strongly suggest that these bands are a premonitory "indication" of this spinel. At higher oxidation temperature, i.e. 510°C, no fine structure is observed in the spectrum (Fig. 9, curve e), indicating that the spinel is disordered as already reported by Jarrige (*15*), whereas a new absorption band centered at about 590 cm^{-1} is present which is likely associated with the formation of α-Mn_2O_3 (Fig. 9, curve f) resulting in the γ-$Mn_2O_3 \rightarrow \alpha$-$Mn_2O_3$ transition.

For comparison, the oxidation kinetic curves for samples with high Mn content ($x = 0.45$ and $x = 0$) are given in Figs. 10 and 11. Clearly, the oxidation mechanism is changing since the Δm against time plots are sigmoidal, indicating a nucleation-growth mechanism (*12*). This can be related to the formation of α-Mn_2O_3 from the beginning of the oxidation reaction by reason of equilibrium associated with the lower proportion of spinel phase. In the X-ray diagram the peaks typical of α-Mn_2O_3 are detected. For composition $x = 0.45$, the amount oxidized during the sigmoidal branch and indicated by an arrow corresponds to that observed in nonisothermal conditions and the oxidation mechanism may be thus explained by Reaction (3). The additional mass gain is associated with the oxidation of Mn^{3+} ions into Mn^{4+} ions. Since α-Mn_2O_3 appears as a second phase, we may conclude that all Mn^{4+} ions have been accommodated in the spinel-type structure according to the following proposed reaction:

$$2x/3(Cu^{+})_A(Cu^{2+}_{0.5}Mn^{4+}_{1.5})_B O^{2-}_4 + (3 - 2x)/2Mn^{3+}_2O^{2-}_3 + y/4O_2 \rightarrow (3 - 2x - y)/2\alpha\text{-}Mn_2O_3 + t/24(Cu^{+}_{16x/t}Cu^{2+}_{8x/t}Mn^{4+}_{24(x+y)/t\square\beta})O^{2-} \quad (7)$$

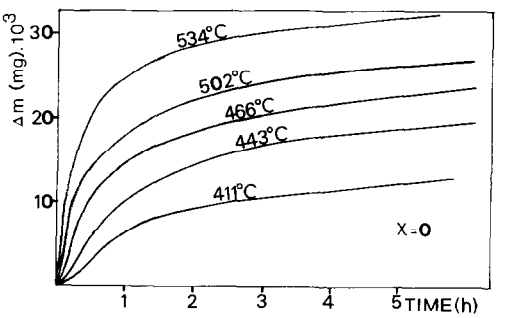

FIG. 11. Kinetic curves, $\Delta m = f(t)$, for spinel with $x = 0$.

For $x = 0$, no significant reoxidation of Mn^{3+} ions is expected to occur because to the absence of the spinel phase.

Conclusion

During this work we have tried to establish if there is a correlation between the cationic distribution and the reactivity in the oxygen of copper manganite spinels $Cu_xMn_{3-x}O_4$ ($0 < x < 1$). The oxidation temperatures are related to the content of Cu^+ and Mn^{2+} ions on tetrahedral sites and the phases formed are in agreement with the fact that, for spinels rich in copper ($x > 0.70$), the copper, by decreasing the oxidation temperature, may permit the existence of cation-deficient metastable spinels below 450°C. In this case the kinetic would be controlled by a diffusion law. It is proposed that the cation-deficient spinel has a formula similar to the ordered spinel $Cu_{1.5}Mn_{1.5}O_4$ with the cation distribution

$$t/24(Cu^+_{16x/t})_A(Cu^{2+}_{8x/t}Mn^{4+}_{24(x+y)}/_{t\square 3y/t})_BO^{2-}$$

and that this spinel was accompanied by a manganese rich spinel like γ-Mn_2O_3.

Significant changes in the oxidation behavior are observed for copper content below $x = 0.70$, in particular a reaction rate controlled by a nucleation-growth mechanism induced by the precipitation of α-Mn_2O_3.

References

1. S. K. KSHIRSAGAR, *J. Phys. Soc. Jpn.* **27,** 1164 (1968).
2. G. T. BHANDAGE AND H. V. KEER, *J. Phys. C; Solid State Phys.* **9,** 1325 (1976).
3. S. BALIGA AND A. L. JAIN, *Mater. Lett.* **9,** 180 (1990).
4. C. D. SABANE, A. P. B. SINHA, AND A. B. BISWAS, *Indian J. Pure Appl. Phys.* **4,** 187 (1966).
5. C. D. SABANE, V. R. TARE, AND A. P. B. SINHA, *Indian J. Pure Appl. Phys.* **5,** 213 (1967).
6. S. SUSEELA AND A. P. B. SINHA, *Indian J. Pure Appl. Phys.* **11,** 112 (1973).
7. E. JABRY, G. BOISSIER, A. ROUSSET, R. CARNET AND A. LAGRANGE, *J. Physique* **47**(C1) 843 (1986).
8. J. P. CAFFIN, A. ROUSSET, R. CARNET, AND A. LAGRANGE, *in* "High-Tech Ceramics" (P. Vincenzini, Ed.), p. 1743, Elsevier, Amsterdam (1987).
9. S. VEPREK, D. L. COCKE, S. KEHL AND H. R. OSWALD, *J. Catal.* **100,** 250 (1986).
10. L. S. PUCKHABER, H. CHEUNG, D. L. COCKE, AND A. CLEARFIEL, *Solid State Ionics* **32/33,** 206 (1989).
11. B. GILLOT, M. KHARROUBI, R. METZ, R. LEGROS, AND A. ROUSSET, *Phys. Status Solidi A,* in press.
12. B. GILLOT, M. EL GUENDOUZI, M. KHARROUBI, P. TAILHADES, R. METZ, AND A. ROUSSET, *Mater. Chem. Phys.* **24,** 199 (1989).
13. R. METZ, J. P.CAFFIN, R. LEGROS, AND A. ROUSSET, *J. Mater. Sci.* **24,** 83 (1989).
14. B. GILLOT, M. EL GUENDOUZI, P. TAILHADES, AND A. ROUSSET, *React. Solids* **1,** 139 (1986).
15. J. JARRIGE AND J. MEXMAIN, *Bull. Soc. Chim. Fr.* **9–10,** 363 (1980).
16. R. E. VANDENBERCHE, G. G. ROBBRECHT, AND V. A. M. BRABERS, *Phys. Status Solidi A* **34,** 583 (1976).
17. B. GILLOT, *Mater. Chem. Phys.* **10,** 384 (1984).
18. W. B. WHITE AND B. A. DEANGELIS, *Spectrochim. Acta* **23A,** 985 (1967).
19. A. D. D. BROEMME AND Y. A. M. BRABERS, *Solid State Ionics* **16,** 171 (1985).
20. G. BLASSE, *Sol. State Commun.* **3,** 67 (1965).
21. R. E. VANDENBERCHE, E. LEGRAND, D. SCHEERLINCK, AND V. A. M. BRABERS, *Acta Crystallogr. Sect. B* **32,** 2796 (1976).
22. J. PATTANAVAK AND Y. SITAKARA RAO, *Thermochim Acta* **153,** 193 (1989).